ELSEVIER

Catalysis Today 67 (2001) 257–272

CATALYSIS TODAY

www.elsevier.com/locate/cattod

CVD preparation of catalytic membranes for reduction of nitrates in water

Kristian Daub [a,1], Volker K. Wunder [a,1], Roland Dittmeyer [b,*]

[a] *Universität Erlangen-Nürnberg, Lehrstuhl für Technische Chemie I, Egerlandstraße 3, 91058 Erlangen, Germany*
[b] *DECHEMA e.V., Karl-Winnacker-Institut, Theodor-Heuss-Allee 25, 60486 Frankfurt am Main, Germany*

Abstract

A catalytic membrane contactor for selective hydrogenation of nitrate in water to nitrogen is discussed as a promising new approach to develop a technically feasible catalytic process for nitrate reduction from ground and surface water. Metal organic chemical vapour deposition (MOCVD) was used to place catalytically active metals, i.e., palladium and tin, inside the porous top-layer of asymmetric ceramic membranes (e.g. alumina) with different pore sizes and thicknesses of the top-layer. The influence of the membrane properties, i.e., the material, pore size and thickness of the catalytic layer, and the influence of the MOCVD process parameters on the deposition of the metals was studied and catalytic membranes with different palladium loading and palladium/tin ratio were prepared. These membranes were characterised with respect to the pore structure and the distribution of the active metals. Their catalytic performance in the hydrogenation of nitrate in water was investigated in a laboratory stirred tank membrane reactor under continuous flow conditions to explore the influence of important process parameters. The results show that the catalytic membranes offer a high activity and a fair selectivity to nitrogen which may be further improved by an optimisation of the preparation procedure.

Keywords: Catalytic membrane; Membrane reactor; MOCVD; Palladium catalyst; Nitrate reduction

1. Introduction

The concentration of nitrate in ground water exceeds the tolerance limit of 50 mg/l set by the European Drinking Water Directive in many areas throughout Europe and in many other regions world-wide. The main source of nitrate contamination is the excessive usage of nitrogen fertilisers. Nitrate, or rather its degradation product nitrite, is suspected to cause serious diseases, i.e., blue baby syndrome and cancer [1]. Various established processes are available for denitrification of water supplies, i.e., ion exchange, biological denitrification, and membrane desalting by reverse osmosis or electrodialysis [2]. However, these techniques usually need a post-treatment of the effluents, or they cannot easily be handled, or they are costly.

Catalytic hydrogenation of nitrate on bimetallic Pd-based catalysts has been proposed in 1989 by Vorlop and co-workers [3,4] as a new method for nitrate removal from drinking water with promising advantages over the conventional techniques in terms of lower waste generation and higher space time yield. Just as biological denitrification catalytic reduction is capable of removing nitrate from the environment in a sustainable manner, i.e., not to shift the problem by separation or concentration. At the same time it is much faster and less delicate in operation [4]. However, the main problem lies in the difficulty to

* Corresponding author. Tel.: +49-69-7564-428; fax: +49-69-7564-388.
E-mail address: dittmeyer@dechema.de (R. Dittmeyer).
[1] Fax: +49-9131-8527421.

0920-5861/01/$ – see front matter
PII: S0920-5861(01)00313-3

Nomenclature

c_i	concentration of species i in the reactor (mmol/l)
$c_{i,0}$	concentration of species i in the feed (mmol/l)
d_i	inner diameter (alumina ring) (mm)
d_o	outer diameter (alumina ring) (mm)
d_p	pore diameter (nm)
h	thickness (alumina ring) (mm)
m_{Pd}	mass of palladium in the catalytic layer (mg)
M_{NO_3}	molar weight of nitrate (mg/mmol)
n_i	mole flow of species i in the product (mmol/h)
$n_{i,0}$	mole flow of species i in the feed (mmol/h)
q	volumetric flow rate (l/h)
R_i	rate of consumption or formation of species i (mmol/l h)
$R_{NO_3^-}$	specific nitrate removal rate defined by Eq. (1) (mg/mg Pd h)
$S_{i,N}$	molar selectivity to species i (based on nitrogen) (%)
V_R	reactor volume (liquid) (l)
X	conversion of nitrate (%)
$Pd(hfa)_2$	palladium(II) hexafluoroacetylacetonate
$Sn(hfa)_2$	tin(II)hexafluoroacetylacetonate

Greek Symbol

τ	residence time (h)

control the activity and selectivity of the catalyst on a technical scale so that incomplete hydrogenation to nitrite and over-hydrogenation to ammonium are both avoided. Nitrite and ammonium face a much stricter limit of 0.1 and 0.5 mg/l, respectively [1].

Supported palladium catalysts with copper or tin acting as promoter have been identified to be the most suitable systems for reduction of nitrate in aqueous solutions [5–9]. Fig. 1 shows a simplified reaction scheme [10]. Nitrate is reduced to nitrogen via several steps involving nitrite, NO, and N_2O as intermediate products. The undesired by-product ammonium is formed in a side reaction claimed to start from surface-NO. The first reaction step, the reduction of nitrate to nitrite, takes place on palladium only in

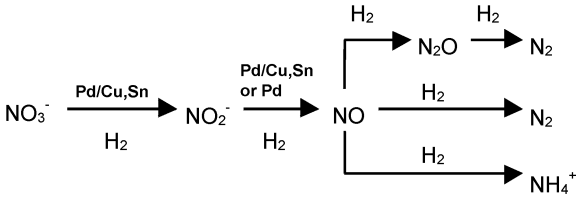

(1) $NO_3^- + H_2 \rightarrow NO_2^- + H_2O$

(2) $NO_2^- + 0.5\ H_2 \rightarrow NO + OH^-$

(3) $2\ NO + H_2 \rightarrow N_2O + H_2O$ and: $N_2O + H_2 \rightarrow N_2 + H_2O$

$2\ NO + 2\ H_2 \rightarrow N_2 + 2\ H_2O$

$NO + 2.5\ H_2 \rightarrow NH_4^+ + OH^-$

Fig. 1. Hypothetical reaction scheme and equations of catalytic hydrogenation of aqueous nitrate on Pd–Cu and Pd–Sn catalysts [10].

presence of a second metal, whereas no such promoter is necessary for the subsequent reduction of nitrite to nitrogen and ammonium [4,11]. Activity and selectivity are severely affected by the reaction conditions, i.e., first of all by the pH value, the hydrogen concentration, the temperature, and the contact time. Moreover, the palladium loading and the ratio of palladium versus promoter is important [12].

Despite large efforts in catalyst development over the past 10 years catalytic nitrate reduction still has problems with the formation of ammonium as a result of over-hydrogenation. So far, the transfer of the preparation method optimised for powder-type materials (2–3 μm particle size) to catalyst supports that can be applied on a technical scale was not successful [3,4,13,14]. Pore diffusion limitation inside the catalyst particles is responsible for a local increase of the pH value, which decreases the activity and the selectivity to nitrogen [5]. Various attempts have been made to overcome this problem: cross flow operated polyetherimide membranes with built-in catalyst particles [15], polymer hollow fibres packed with powder catalysts [16], hydrogel encapsulated catalysts [17], and macroporous alumina membranes with Pd–Cu incorporated as active species [18]. None of these methods reached the very high selectivity to nitrogen required without substantially decreasing the activity.

We have recently reported the use of asymmetric meso-/macroporous ceramic membranes containing Pd–Cu or Pd–Sn catalysts in the top-layer [19,20].

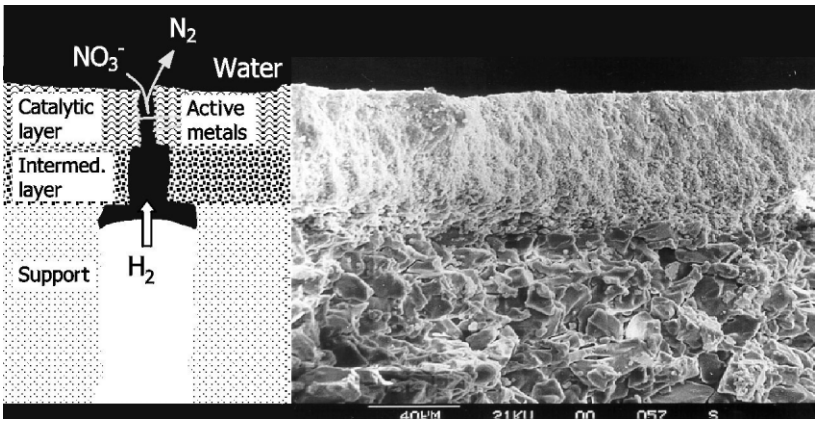

Fig. 2. Schematic of the catalytic membrane. The thickness of the catalytic layer (uppermost layer) is of the same order as the particle size of a powder catalyst. The gas side is operated at a pressure between the bubble point pressure of the support and that of the catalytic layer. The liquid side is maintained at ambient pressure.

Such a system offers an interesting perspective in that respect that the ceramic membrane can act both as catalyst support and as hydrogen dosing unit. Fig. 2 explains the working principle of the catalytic membrane. The active layer is in contact with the nitrate solution, which is wetting the membrane surface, and hence penetrates into the pore structure. On the support side hydrogen is supplied. The pore size of the support is well above the pore size of the top-layer. By setting the gas side pressure within a working window defined by the bubble point pressure of the membrane support as the lower limit and the bubble point pressure of the top-layer as the upper limit, it is possible to establish the gas–liquid interface close to the top-layer carrying the active metals. Right at the gas–liquid interface the gas side pressure equals the liquid side pressure plus the capillary pressure of the liquid filling the pores.

The benefits are not only a high activity thanks to the short diffusion path length but also a simple and compact reactor design. The catalytic membrane enables an efficient three-phase contact between gaseous hydrogen, solvated nitrate ions, and the active surface. The pore size of the catalytic layer can be adjusted in the mesoporous or macroporous range according to the needs of the reaction, with a narrow pore size distribution. Moreover, the membrane catalyst concept allows a tuning of the reaction rate by adjusting the hydrogen pressure to suit variable operating situations, i.e., different nitrate concentration, rate of water flow, and so on [19,20]. Finally, scale-up appears to be straight forward.

2. Experimental

2.1. Membrane supports

Tubular ceramic micro/ultrafiltration membranes obtained from HITK e.V., Hermsdorf (Germany), were used as starting materials. The membranes have an outer diameter of 10 mm, an inner diameter of 7 mm, and the usual asymmetric structure consisting of a coarse α-alumina support, intermediate layers with graded pore size (α-alumina), and a thin top-layer of γ-alumina, α-alumina, titania or zirconia on the outer side. In this paper, we report results obtained on α-alumina layers with different pore diameters (60, 100, 200 and 400 nm) and thicknesses (8–42 μm).

2.2. Metal organic chemical vapour deposition

For deposition of palladium and tin in the pore structure of the membrane top-layer both MOCVD and an impregnation–calcination–reduction method were applied. In this paper, we discuss only the results of the MOCVD route, which was set up following information from literature [21–23]. The deposition was carried out in a discontinuously working horizontal

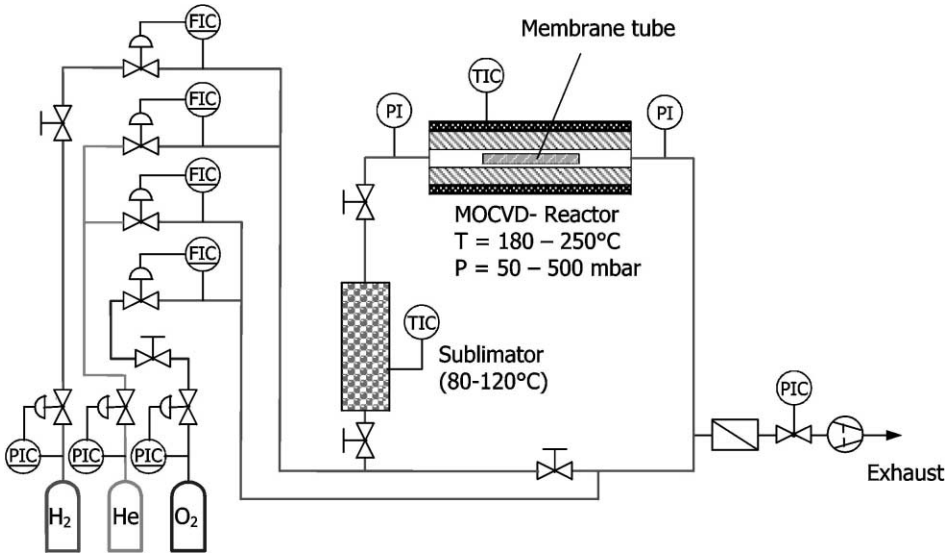

Fig. 3. Schematic of the MOCVD reactor setup. TI, PI and FI indicate temperature, pressure, flow indicators. TIC, PIC and FIC denote temperature, pressure, flow controllers.

hot wall reactor made of a quartz tube of 30 cm length and 16 mm diameter. Fig. 3 shows a schematic of the CVD setup. Feeding of the metal organic precursors was achieved using a carrier gas saturated with the precursor by passing a heated bed of quartz beads containing a given amount of the solid precursor. Palladium(II)hexafluoroacetylacetonate ($Pd(hfa)_2$, CAS-No. [64916-48-9]) and Tin(II)hexafluoroacetylacetonate ($Sn(hfa)_2$, CAS-No. [51319-99-4]) were used as precursors because of the higher vapour pressure compared to the low fluorinated compounds. Both chemicals were purchased from ABCR GmbH KG, Karlsruhe (Germany), the purity was $\geq$99.0% in case of $Pd(hfa)_2$ and $\geq$99.9% for $Sn(hfa)_2$. The vapour pressure of the precursors was determined by thermogravimetric analysis.

Prior to the membrane preparation the kinetics of palladium deposition from $Pd(hfa)_2$ on dense α-alumina rings ($d_i = 5$ mm, $d_o = 10$ mm, $h = 0.9$ mm) were studied. A total of 15 rings were placed in the isothermal zone in the centre line of the quartz tube on a holder with 10 mm spacing between the individual rings. The metal deposition rate was calculated from the weight increase of the individual rings per surface area and time. In this way, it was possible to determine the variation of the deposition rate along the reactor axis. The target was to identify a set of operating conditions which guarantee a sufficiently high but more or less uniform deposition rate along the reactor so that regular metal concentration profiles could be expected when preparing catalytic membranes. The similar decomposition behaviour of different metal hexafluoroacetylacetonates allowed to use, in a first assumption, the determined deposition conditions for the palladium system also for the deposition of tin.

Although the deposition on porous substrates is more complicated in that it involves also diffusion in the pore structure, the results obtained with non-porous rings provide useful information about suitable operating conditions for the preparation of catalytic membranes. The deposition in the membranes shall be limited to the thin top-layer (10–50 μm) beneath the external membrane surface. This layer has a limited inner surface area, i.e., relatively large pores ($d_p \approx$ 60–400 nm). If the CVD conditions are properly adjusted so that the metal deposition rate shows no significant axial gradients, it can be assumed that intra-pore gradients in the range of the top-layer thickness play only a minor role.

The main variables controlling the metal deposition rate are the precursor concentration, which is controlled by the sublimator temperature, the reactor

Table 1
Selected operating parameters for deposition of palladium and tin in the top-layer of the asymmetric membranes

Parameters	Pd	Sn
Reactor pressure (absolute) (mbar)	500	500
Reactor temperature (°C)	250	250
Sublimator temperature (°C)	80	120
Precursor concentration ($Me(hfa)_2$) calculated from the vapour pressure given by the sublimator temperature ($\mu mol\,m^{-3}$)	77	2.5
Helium flow rate ($\times 10^6$ ($m^3\,s^{-1}$)[a])	1.58	0.83
Hydrogen flow rate ($\times 10^6$ ($m^3\,s^{-1}$)[a])	–	0.83

[a] STP.

temperature, and the reactor pressure. The effect of the precursor concentration on the palladium deposition rate was investigated at $Pd(hfa)_2$-concentrations in the range of 20–600 $\mu mol\,m^{-3}$ in helium at a fixed pressure of 500 mbar. The influence of the reactor temperature was studied from 225 to 375°C, the reactor pressure was changed between 125 and 950 mbar. The helium carrier gas flow rate was fixed at $1.58 \times 10^{-6}\,m^3\,s^{-1}$ (STP) during all experiments, except those with varying reactor pressure. In the isothermal zone of the reactor (40–240 mm) the measured axial temperature gradient was generally less than $3\,K\,cm^{-1}$.

For the deposition of the metals in the porous membranes both faces were sealed to ensure that the precursor penetrates into the pore-structure from the outer side of the membrane tubes only. The membranes were placed in the isothermal section of the CVD reactor. Table 1 gives an overview of the operating conditions which were identified as a reasonable choice between high and uniform metal deposition rate. The desired metal content of the membranes was adjusted by variation of the deposition time. Note that the deposition of palladium was carried out with pure helium carrier gas whereas in case of the deposition of tin a mixture of helium and hydrogen was used to ensure that tin is received in reduced form, so that no subsequent treatment of the catalytic membranes is necessary.

2.3. Characterisation of the membrane structure and composition

The structure and composition of the prepared catalytic membranes was characterised by various techniques. The pore size distribution of the top-layer was measured by capillary flow porometry (Porous Materials, Ithaca, NY) before and after introducing the active metals. In this method, the flow through the membrane is recorded as a function of the pressure difference in dry state and completely wetted by a wetting agent with known surface tension. The measuring principle is based on the fact that the differential pressure over the membrane must exceed the capillary pressure in a wetted pore of a given diameter before gas flow through this pore can occur. This leads to a deviation between the dry curve and the wet curve. At differential pressures below the bubble point of the membrane there is no gas flow at all. Above the bubble point pressure the wet curve is gradually approaching the dry curve from the bottom with increasing pressure difference. By analysing both signals it is possible to determine the gas flow as a function of the size of the pores. Note that not the volume-based mean pore diameter is relevant but the size of the bottlenecks of the pores. The primary information is the so-called cumulative filter flow. Derivation of this curve yields the differential filter flow which can be scaled to give a pore-size distribution showing the variation of the size of the narrowest cross-sections of the pores [24]. For asymmetric (composite) membranes this method offers the advantage of analysing only the relevant part of the membrane, that is the fine porous top-layer. Galden HT 230 by Ausimont S.p.A., a perfluorinated polyether normally used as a heat transfer liquid, was employed as wetting agent. This substance (CAS-No. [69991-67-9]) has a low vapour pressure and a low surface tension of $20\,mN\,cm^{-1}$ (25°C), which enables reliable measurements down to pore diameters around 15–20 nm. It was purchased from Ausimont Deutschland GmbH, Eschborn/Ts. (Germany).

The distribution of palladium and tin over the membrane cross-section was analysed by electron probe microanalysis (EPMA) with wavelength-based detection (WDX). For this purpose cross-sectional cuts of the membrane top-layers, taken at different radial and axial positions, were prepared by metallographic methods. The EPMA instrument was operated at a beam diameter expansion of about 2 μm. The penetration depth of the electron beam was estimated to 3–4 μm. Line scans were performed from the outer membrane surface to a depth of 50–60 μm with a point to point distance of 2 μm.

To determine the average metal cluster size, X-ray diffraction with line broadening analysis (XRD), pulse chemisorption of carbon monoxide, and in some cases transmission electron microscopy (TEM) were applied.

2.4. Catalytic testing of the membranes

The catalytic properties of the membranes were tested in a stirred-tank membrane reactor operated in continuous mode (cf. Fig. 4). In this set-up the membranes are immersed in the liquid phase (ca. 780 ml) which is well mixed by a magnetically coupled blade stirrer or impeller. The mixing of the liquid phase was checked by performing tracer experiments (displacement technique). This allowed to verify that for liquid residence times above 30 min, the reactor can be treated as an ideal stirred tank reactor (CSTR). Practically, no deviation of the measured residence time distribution from the theoretical CSTR-curve was found under these conditions. Neither bypassing nor significant dead volume could be detected within the limits of the experimental error. This enables a direct calculation of the rate of consumption or formation of the various species from the concentration change between inlet and outlet of the reactor divided by the residence time:

$$R_i = \frac{c_i - c_{i,0}}{\tau} \tag{1}$$

The residence time τ is given by the reactor volume (liquid) divided by the volumetric flow rate:

$$\tau = \frac{V_R}{q} \tag{2}$$

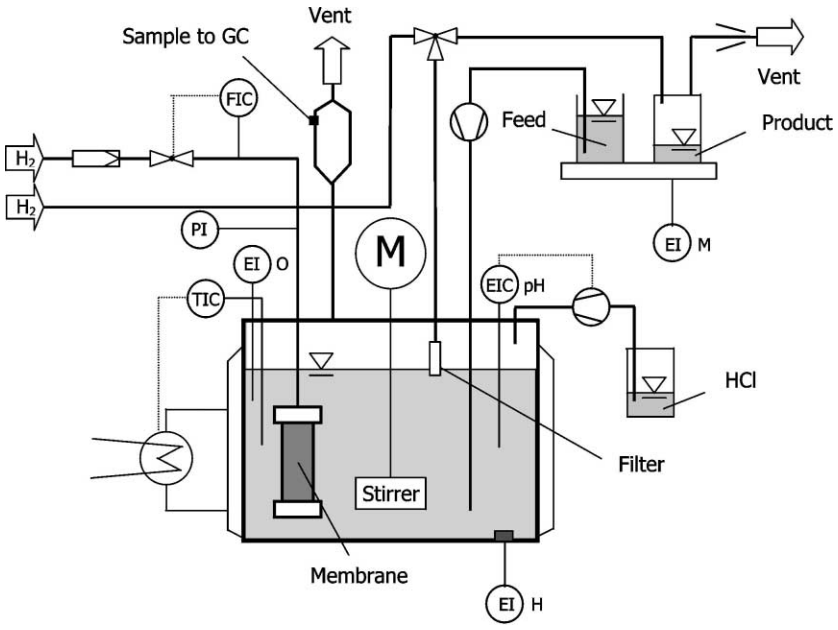

Fig. 4. Basic layout of the laboratory CSTR membrane reactor. GC: gas chromatograph. M: motor. EIC pH: pH-control unit (dosage of HCl). EI H: electrochemical sensor for dissolved hydrogen. EI O: opto-chemical sensor for dissolved oxygen. EI M: balance. For other symbols refer to Fig. 3.

Eq. (1) is obtained directly from the CSTR mass balance by assuming a negligible change of volume, i.e., that the volumetric inlet flow rate equals the outlet flow rate.

Putting $i = NO_3^-$ in Eq. (1), multiplying with the molar weight of nitrate, and dividing by the mass of palladium present in the catalytic layer, yields the specific nitrate removal activity which is used later on in the discussion of the catalytic performance.

$$R^{\mathrm{m}}_{NO_3^-} = \frac{M_{NO_3^-}}{m_{\mathrm{Pd}}} \frac{(c_{NO_3^-} - c_{NO_3^-,0})}{\tau} \tag{3}$$

It is emphasised that the quantity $R^{\mathrm{m}}_{NO_3}$ in Eq. (3) in general does not represent the intrinsic activity of the catalytic membranes. It is true that the concentration in the bulk liquid is constant (well mixed) but no information is available about possible concentration gradients inside the catalytic layer and in the adjacent fluid film on the membrane surface. Therefore $R^{\mathrm{m}}_{NO_3}$ is an effective reaction rate which can be influenced to some extent by diffusion of the reactants.

The membrane is connected with the hydrogen supply line at one end. The other end is sealed. Gas feeding to the membrane is achieved by thermal mass flow controllers, and the gas pressure in the membrane is recorded. The reactor vessel consists of a double-walled glass jacket fixed between two metal flanges. The reactor temperature is regulated by a temperature-controlled shell-side liquid. The reactor is equipped with an electrochemical hydrogen sensor integrated in the bottom flange and a fibre-optic oxygen sensor immersed in the liquid to detect the concentration of dissolved hydrogen and oxygen. The liquid feed is metered by a pulse-free peristaltic pump. A vacuum pump is used to withdraw the product stream by evacuation of the product tank. Before entering the connecting pipe, the product stream passes a fine sintered metal filter where particles are retained. Backflushing of this filter is possible by applying hydrogen pressure.

The volumetric feed flow rate must match the product flow rate to keep the liquid level in the reactor constant. This is monitored by a balance recording the total weight of the feed and product tanks. During an experiment, the vacuum pump is adjusted to keep the reading of the balance constant. A pH-controller with dosage of hydrochloric acid is available to maintain a constant pH during the reaction. Samples of the gas atmosphere in the reactor can be taken by a gas syringe, they are analysed in a gas chromatograph. The principal analytical instruments are two ion chromatographs (Metrohm AG, Filderstadt/Germany) which serve to determine the concentration of the anions (nitrate, nitrite) and cations (ammonium), respectively. The operating parameters of the ion chromatographs are summarised in Table 2.

Besides the specific nitrate removal activity defined by Eq. (3), the conversion of nitrate

$$X_{NO_3^-} = \frac{c_{NO_3^-} - c_{NO_3^-,0}}{c_{NO_3^-,0}} \times 100\,(\%) \tag{4}$$

and the molar selectivity to nitrogen, nitrite and ammonium (based on nitrogen atoms)

$$S_{i,\mathrm{N}} = \frac{n_i - n_{i,0}}{n_{NO_3^-,0} - n_{NO_3^-}} \frac{\nu_i}{1} \times 100\,(\%) \tag{5}$$

are used to characterise the catalytic performance of the membranes. The quantity ν_i in Eq. (5) denotes the number of N-atoms in species i.

Table 2
Operating parameters of the ion chromatographs

	Anions	Cations
Column	Metrosep anion 2	Metrosep cation 1–2
Filling material	Polymethacrylate with quaternary ammonium groups	Polybutadiene–maleic acid on silica gel
Length/diameter	75 mm/4.6 mm	125 mm/4.0 mm
Eluent	1.3 mmol/l Na_2CO_3, 2.0 mmol/l $NaHCO_3$	4 mmol/l tartaric acid, 1 mmol/l dipicolinic acid, 1 mmol/l 18Crown-6 ether
Flow rate	0.8 ml/min	1.0 ml/min
Column pressure	42 bar	60 bar
Chemical suppression	Yes	–

3. Results and discussion

3.1. Influence of the MOCVD process parameters on the deposition of palladium from palladium(II)hexafluoroacetylacetonate on α-alumina rings

Above 225°C a measurable amount of palladium is deposited on the α-alumina rings. In the temperature range between 225 and 250°C an exponential increase of the deposition rate is found indicating control of the process by the surface chemical reaction. From 250 to 275°C the increase of the deposition rate tends to become linear, at higher temperatures it starts levelling off and reaches a maximum around 350°C. The decrease of the temperature influence on the deposition rate points to growing mass transport limitation in this region. A further increase of temperature causes a reduction of the deposition rate, which is attributed to the onset of homogeneous gas phase reactions, i.e., thermal decomposition of the precursor under formation of metal and soot particles. In addition, a high amount of palladium is deposited on the tube wall in the entrance of the reactor under these conditions.

Fig. 5 shows measured profiles of the palladium deposition rate at various temperatures. Based on these results a reactor temperature of 250°C seemed to be a reasonable choice balancing the demands for a high deposition rate, as uniform as possible distribution of the metals, and acceptable precursor efficiency.

In the chemically controlled regime being present at reactor temperatures of 250°C or below, the palladium deposition rate obeys a complex hyperbolic rate law. Initially, the deposition rate increases proportionally to the partial pressure of the precursor but levels off gradually and is even reduced at high concentrations. Adsorption of the precursor and the decomposition products is responsible for this behaviour. For the $Pd(hfa)_2$-system the maximum deposition rate was found at a precursor concentration of 45 $\mu mol\,m^{-3}$. To achieve a reasonable high precursor efficiency, the precursor concentration should not exceed 70–80 $\mu mol\,m^{-3}$, which means a maximum sublimator temperature of 80°C.

The effect of the reactor pressure was studied in the range between 125 and 950 mbar at a reactor temperature of 275°C and a fixed sublimator temperature of 80°C, giving a constant precursor concentration of 77 $\mu mol\,m^{-3}$. In the low pressure range, a small increase of the deposition rate with increasing pressure was noticed at constant precursor concentration. Above 500 mbar no significant influence of the reactor pressure could be detected.

The morphology and the composition of the palladium layers on the ceramic rings proved to be merely influenced by the process conditions. The morphology shows a macroscopic smooth coating

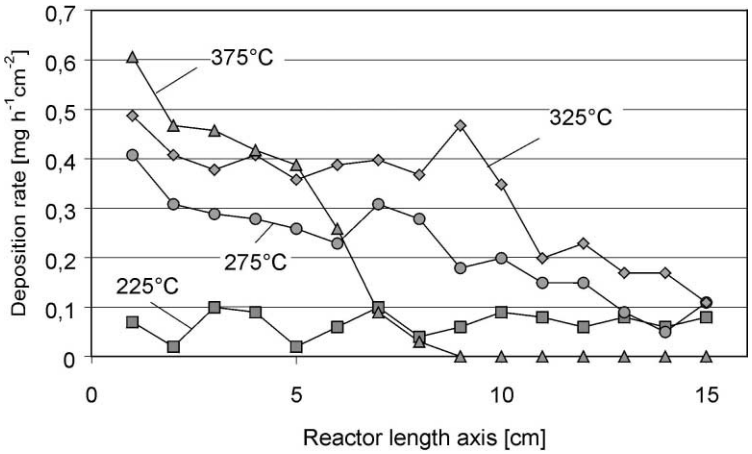

Fig. 5. Influence of the reactor temperature on the axial profile of the palladium deposition rate determined from the weight increase of dense α-alumina rings placed in the CVD reactor. Pressure: 500 mbar. $Pd(hfa)_2$-concentration: 77 $\mu mol\,m^{-3}$ ($T_{Subl.} = 80°C$). Helium flow rate: $1.58 \times 10^{-6}\,m^3\,s^{-1}$.

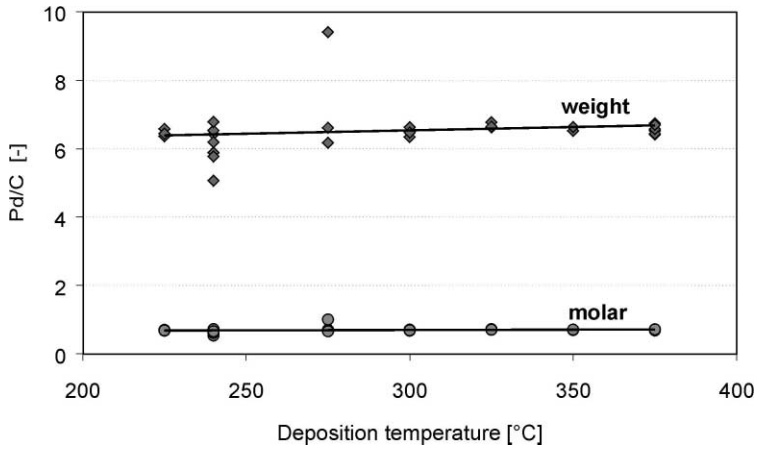

Fig. 6. Influence of the reactor temperature on the Pd:C ratio of the deposited palladium films. Reactor pressure: 125–950 mbar. Precursor concentration: 20–600 μmol m^{-3}.

with microscopic roughness. The composition of the layers was analysed by Auger-Electron-Spectroscopy (AES). Palladium and carbon were identified after sputtering the surface with an argon ion beam (60 nm). Carbon originates obviously from fragments of the organic precursor. It was found that the Pd:C atomic ratio of the films remains nearly constant at values around 0.65–0.75 in the investigated range of pressure, temperature, and precursor concentration (cf. Fig. 6). The carbon content of the palladium films might be due to the catalytic activity of palladium for dehydrogenation and decomposition of the precursor ligands, which in the end leads to the formation of carbon deposits on the palladium surface.

3.2. Preparation of membrane catalysts by MOCVD of palladium and tin

Various α-alumina membranes with different top-layer thicknesses and pore sizes were modified by depositing palladium and tin in the porous structure. One series of tests was performed on membranes with a top-layer pore diameter of 100 nm and thicknesses varying in the range of 8–42 μm. For a second series, membranes with 60–400 nm pore size and 20 μm thickness of the top-layer were used. Previous investigations had shown that the precursor deposition sequence strongly affects the activity and selectivity of the catalytic membranes for nitrate reduction [20]. Hence, the preferred sequence, i.e., first tin and then palladium, was applied for all experiments. The exact deposition conditions are summarised in Table 2. The metal loading was adjusted by varying the deposition time, the actual metal content was calculated from the weight increase after the deposition without correcting for co-deposition of carbon. This is associated with an over-estimation of the palladium content of 13–17% if one assumes a Pd:C ratio similar to the palladium coating on the dense α-alumina rings. The palladium amount determined this way varied between 5 and 30 mg, which corresponds to 3–11 wt.% related to the mass of the complete top-layer. The tin loading was adjusted and calculated likewise. It varied between 3 and 10 mg.

3.2.1. Metal particle size

The size of the metal particles determines the surface area available for hydrogenation of nitrate. XRD line broadening analysis was performed to determine the metal particle size on samples obtained by scraping off the top-layer from the membranes. Evaluation of the palladium peak at $2\theta = 40.1^\circ$ revealed cluster sizes generally in the range of 7–11 nm depending mainly on the internal surface area of the top-layer, and on a possible temperature treatment. Fig. 7 shows four XRD diffraction patterns of which the first was recorded after preparation and the other three after calcination at different temperatures followed by a

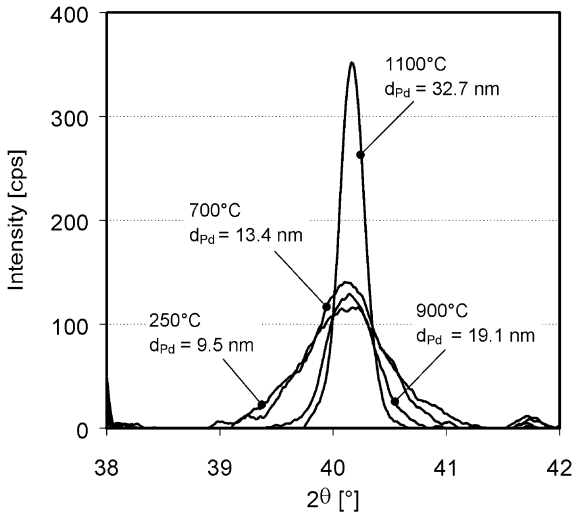

Fig. 7. XRD diffraction patterns (detail) of a catalytic membrane as prepared and after temperature treatment. Pore size: 100 nm. Thickness of top-layer: 20 μm. Analysis of powders scraped off the membranes (catalytic layer). Palladium particle size determined by LBA from the peak at $2\theta = 40.1^\circ$ (Scherrer formula, integral line breadth β_i).

reduction with hydrogen at 150°C. For these measurements a membrane with 100 nm nominal pore size and 20 μm thickness of the top-layer (Pd content ≈ 20 mg) was cut into four pieces which were then temperature-treated in a laboratory oven (air). After the reduction the top-layers were scratched off and the powders were analysed in a powder diffractometer. The changes of the peak shape at $2\theta = 40.1^\circ$ with the calcination temperature are clearly visible. For the fresh membrane a relatively broad peak is found which gets more and more narrowed with higher temperature. The calculation of the mean particle size according to the Scherrer formula gave a value of 9.5 nm for the fresh membrane, 13.4 nm after 700°C, 19.1 nm after 900°C, and 32.7 nm after 1100°C.

As a general rule, for layers with 200 and 400 nm pore diameter a palladium particle size of 10–11 nm was found, whereas for the smaller pore diameters of 60 and 100 nm the indicated cluster size was around 8 nm (cf. Table 3). However, it must be stated that due to the small amount of palladium present in the samples, the determination of the particle size from the diffraction spectra was difficult in many cases, if not impossible.

An alternative method to access the size of the metal particles in the catalytic top-layer is pulse CO-chemisorption which was performed both on membrane pieces of several centimetre length and on samples scraped off from the membranes (top-layer). The evaluation of the data led to the same conclusions as the XRD results, but the method suffers from the same problem, i.e., the low palladium content of the samples. Moreover, the fact that the amount of palladium is not precisely known introduces an additional error in the determination of the palladium particle size by this technique.

To obtain a better impression of the metal particle size TEM investigations were carried out on selected membranes. The samples were prepared once more by scraping off the membrane top-layers. The resulting powder was ground to a particle size suitable for investigation in the transmission electron microscope, i.e., in the range of 50–100 nm. Fig. 8 shows a representative example of the TEM photographs. It refers

Table 3
Palladium particle size of catalytic membranes with different thicknesses and pore diameters of the top-layer, determined by XRD line broadening analysis according to the Scherrer formula (Pd-peak at $2\theta = 40.1^\circ$) from powder samples obtained by scraping off the catalytic top-layers

Mean pore diameter of the top-layer (nm)	Thickness of the top-layer (μm)	Estimated internal surface area ($m^2\,g^{-1}$)	Palladium particle size (nm)
100	8	9	8.2
	28		8.0
	42		7.5
60	20	16	8.1
100		9	8.6
200		5	10.2
400		2	10.7

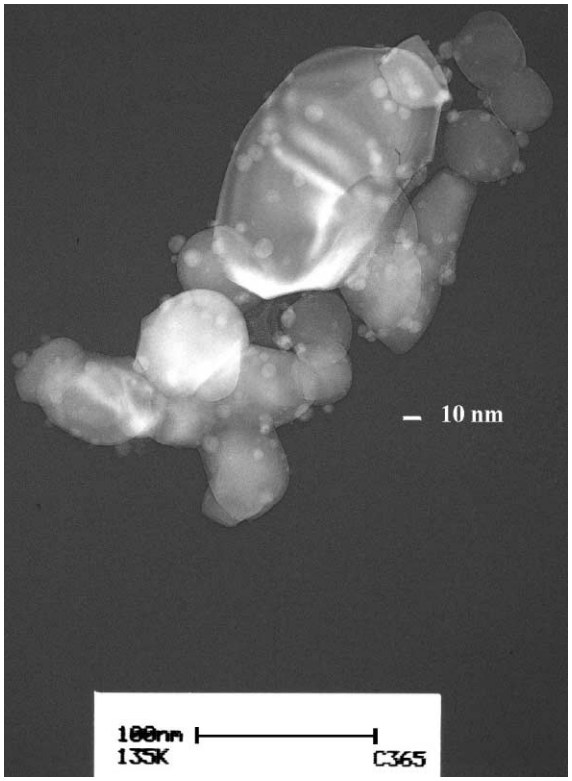

Fig. 8. TEM-photograph of a powder sample scraped off from the top-layer of a catalytic membrane. MOCVD of $Pd(hfa)_2$ and $Sn(hfa)_2$ at the conditions of Table 1. Pore size of the top-layer: 100 nm. Thickness of the top-layer: 20 μm. Small particles represent clusters of the catalytic metals. Large particles represent α-alumina support.

to a membrane with 100 nm pore diameter and 20 μm thickness of the top-layer. The metal clusters on the α-alumina particles are clearly visible. EDX analysis was not performed, so there is no information yet about whether the particles concern palladium or tin (or both). The particle distribution appears more or less uniform. However, a larger number of samples would have to be analysed before general conclusions can be drawn. The size of most of the metal particles is below 10 nm, which is in good agreement with the results of the XRD analysis for this type of membrane (ca. 8 nm). A quantitative analysis of the particle size, e.g. by digital image processing, was not performed due to the limited number of particle images.

3.2.2. Pore structure of the catalytic layer

Capillary flow porometry was performed on some membranes before and after MOCVD to study the modification of the pore structure of the top-layer by deposition of the metal particles. Fig. 9 shows an example of the results obtained by this method. The pore size distribution is related to the flow, not to the pore volume as in the case of mercury porosimetry or gas adsorption measurements. It, therefore, provides information only about what percentage a given effective pore diameter contributes to the total gas flow. No statement is made concerning the absolute value of the gas flow. Note that the narrowest cross-section along the pathway of the gas through a given pore is relevant, not the mean diameter of the pore, because this determines the capillary pressure. Fig. 9 also displays the pore size distribution of a top-layer of the same type of membrane measured by mercury porosimetry. These data were provided by the manufacturer, Inocermic GmbH, Hermsdorf (Germany). Agreement between both methods seems to be reasonable if one considers the different meaning of the pore size according to the deviating measuring

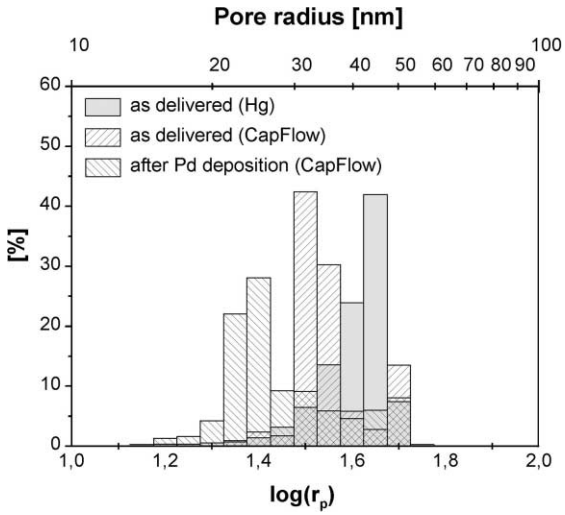

Fig. 9. Pore size distribution of the catalytic top-layer before and after deposition of palladium (MOCVD). Nominal pore diameter: 100 nm. Nominal thickness: 20 μm. Palladium amount: 10 mg on 11 cm tube length (equivalent to 34.5 cm^2). Comparison of capillary flow porometry and mercury porosimetry. Hg porosimetry was carried out by Inocermic GmbH, Hermsdorf (Germany) on a layer coated on a non-porous α-alumina support.

principles. Both curves reveal a narrow pore size distribution. Mercury porosimetry detects a maximum around 45 nm pore radius, whereas the maximum determined by capillary flow porometry lies at 64 nm pore diameter. Keeping in mind that the flow-based method is sensitive to the narrowest cross-section of the pores, it is not surprising that the mean flow pore diameter is smaller than the mean volume pore diameter.

From the comparison of the curves in Fig. 9 it can be seen that after palladium deposition the maximum of the pore size distribution is shifted towards a smaller pore size. The mean pore diameter is reduced from 64 to 48 nm, i.e., by 16 nm. Moreover, the pore size distribution is broadened. These observations are in line with the findings of the other methods, indicating altogether that the deposition by MOCVD leads to metal particles of roughly 10 nm size which are placed irregularly in the pore structure of the membrane top-layer. On the other hand, the influence of the deposition on the overall pore structure is limited. This is confirmed by the fact that the resistance of the membrane to the gas flow is not changed, i.e., the dry curves of the gas flow versus the differential pressure before and after MOCVD fall almost perfectly together.

3.2.3. Metal distribution

The distribution of the metals over the various membrane layers is important because it defines the region where the reactions take place later on. EPMA/WDX was applied to measure the metal concentration profiles across the membrane top-layer. Fig. 10 shows the typical course of the palladium concentration as a function of the distance from the outer surface of the membrane. It is related to a membrane with 100 nm pore diameter and 28 μm thickness of the top-layer. Palladium is detected mainly in the first 50 μm indicating the penetration depth of the precursor during the preparation. The palladium loading decreases from 4.7 wt.% at the outer surface to about 3 wt.% at a depth of 28 μm where the top-layer ends. Further inside the membrane structure the palladium loading drops down to 2.2 wt.% in the intermediate layer, which has a thickness of 15–20 μm, and then quickly to values close to zero in the support at a penetration depth exceeding 50–55 μm. This situation was confirmed to be representative by additional line scans taken at other positions of the membrane.

Calculating the palladium amount from the measured profiles showed that most of the palladium, i.e., 62–94%, is actually located in the top-layer. As an average, this value increases with increasing membrane layer thickness and reduced pore size. Moreover, if scaled by the surface area, which can be determined in a first approximation from the porosity and the mean pore size of the various layers, the palladium profiles become relatively flat (cf. Fig. 10). That is, the data suggest that the deposition rate of palladium is more

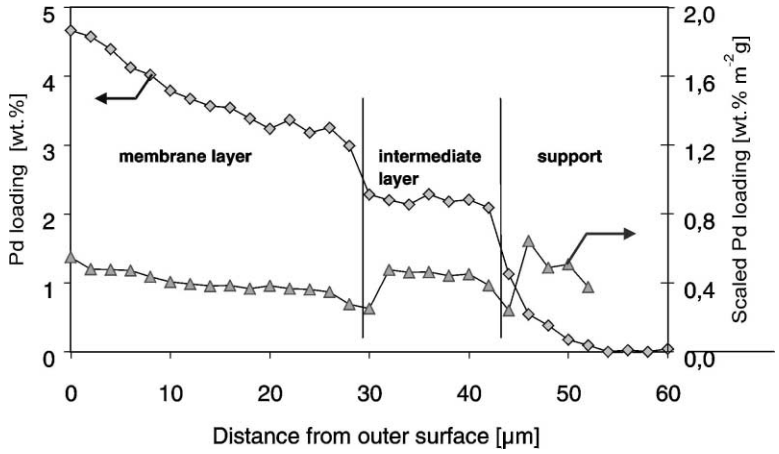

Fig. 10. Typical palladium concentration profile across the asymmetric membrane determined by an EPMA/WDX line scan. Pore size of the top-layer: 100 nm. Thickness of the top-layer: 28 μm. Rhombuses denote weight percent of palladium. Triangles show weight percent of palladium divided by the internal surface area of the layer.

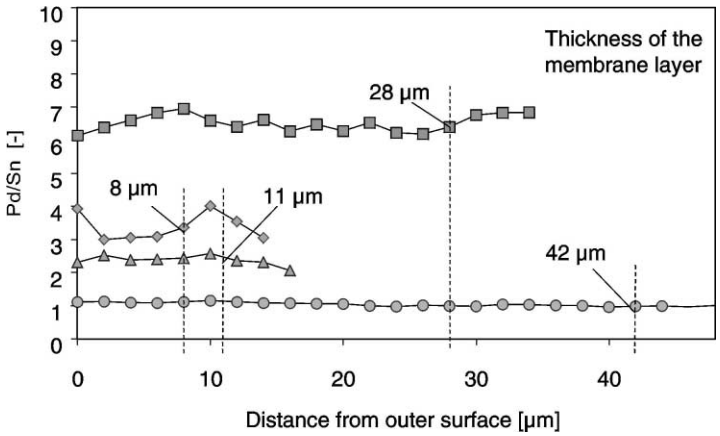

Fig. 11. Pd:Sn atomic ratio in the top-layer and part of the intermediate layer of four different asymmetric membranes, calculated from metal profiles determined by EPMA/WDX line scans. Different palladium and tin loading. Pore size of the top-layer: 100 nm. Thickness of the top-layer: 8–42 μm.

or less proportional to the available surface area, and there is only a moderate influence of diffusion hindrance of the palladium precursor inside the top-layer.

The situation is similar for the deposition of tin. Fig. 11 shows the weight-based ratio of Pd:Sn calculated from the palladium and tin profiles of four different membrane top-layers. Note that the Pd:Sn ratio is constant within the experimental error over the whole depth of the top-layer in all cases. Since the Pd:Sn ratio has a big influence on the activity and selectivity during hydrogenation of nitrate [5], it is important to control this parameter.

Various investigations point to a significant influence of the particle size of powder catalysts on the catalytic performance for hydrogenation of nitrate [5,7,25]. A small particle size is necessary to reduce pore diffusion limitation effects which otherwise limit the activity and the selectivity to nitrogen due to an increased pH value inside the particles. The mean pore diameter of typical powder-type catalyst supports is around 70 Å [7]. In contrast, the pore size of the membranes used in this work is by a factor of 10 higher (i.e., $d_p > 60$ nm). To determine the influence of the top-layer thickness on the preparation and on the catalytic behaviour, membranes with identical pore diameter (100 nm) but different thicknesses of the top-layer were modified by MOCVD. Fig. 12 shows the profiles of the standardised palladium loading of these membranes. Standardised loading here means the loading divided by the loading at the first point of the profile, i.e., close to the outer surface. It was found that the penetration depth of the precursor during MOCVD is influenced by the top-layer thickness. The deposition in the top-layer is favoured with higher thickness of the top-layer. The percentage of the total deposited palladium present in the top-layer increases from 62% at 8 μm thickness to 94% at 42 μm thickness.

3.2.4. Catalytic performance of the membranes in hydrogenation of aqueous nitrate

Investigations on the catalytic performance of the prepared membranes were carried out in the CSTR membrane reactor at standard conditions to enable a correlation of the results with the observations from the membrane characterisation experiments. The dependency of the activity and selectivity on the thickness of the membrane top-layer is illustrated in Figs. 13 and 14. The specific activity observed under typical conditions is generally in the range of 0.8–1.0 mg nitrate converted per milligram palladium and hour for membranes with a top-layer thickness between 8 and 20 μm. Membranes with thicker top-layers show only 20–30% of this activity (cf. Fig. 13). Several factors may contribute to this observation. Most likely, the limited diffusion rate of nitrate or dissolved hydrogen is responsible for a reduction of the catalyst efficiency factor once the

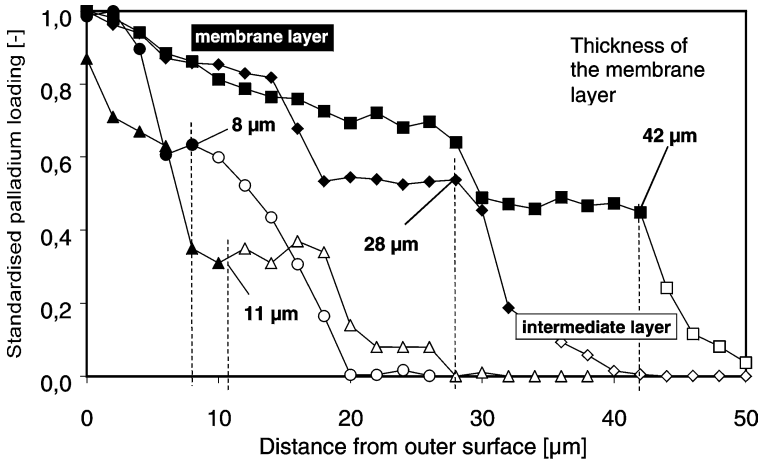

Fig. 12. Palladium concentration profiles across four different asymmetric membranes with varying thickness of the top-layer, determined by EPMA/WDX line scans. Pore size of the top-layer: 100 nm. Each profile is scaled with the palladium concentration detected at the first measurement point (close to the outer surface). Filled symbols indicate the range of the top-layer, open symbols denote the intermediate layer. Dotted lines mark the thickness of the different top layers.

thickness of the top-layer exceeds a critical value. Diffusion hindrance causes a depletion of reactants inside the catalytic layer and hence reduces the overall nitrate conversion rate. However, other reasons are conceivable as well, such as a displacement of the location of the gas–liquid interface with the thickness of the top-layer. This could lead to a situation where the top-layer is not completely wetted and hence a fraction of the deposited metals is not available for the reaction. Additional investigations, both in terms of more extensive experiments and a rigorous simulation taking into account reaction and diffusion inside the membrane are in preparation to clarify this effect.

Fig. 14 illustrates the dependency of the selectivity on the thickness of the top-layer. Generally, the main products of the reaction are nitrogen and ammonium,

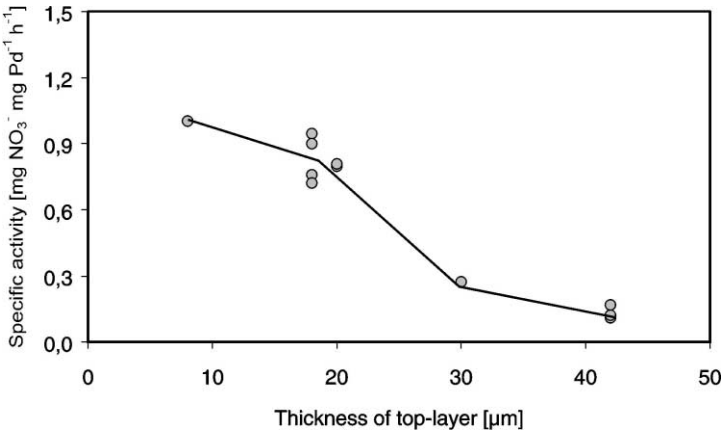

Fig. 13. Influence of the thickness of the top-layer on the specific activity of the membranes for nitrate removal. Pore size of the top-layer (nominal): 100 nm. Reference conditions — gas side hydrogen pressure: 4 bar. pH: 4.7. Temperature: 15°C. Residence time: 60 min.

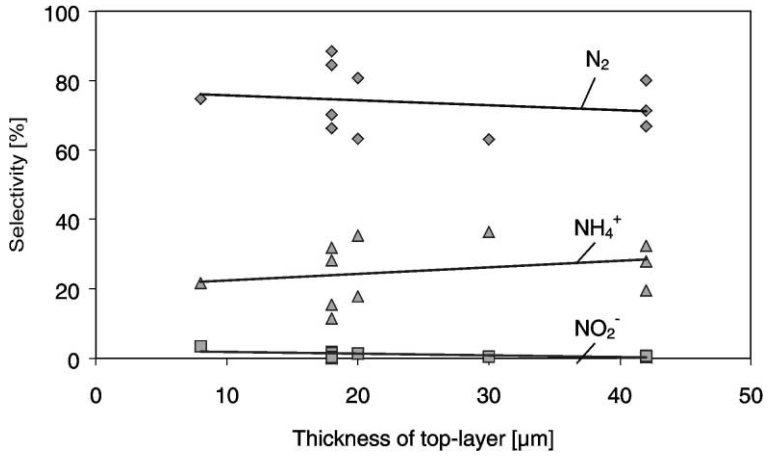

Fig. 14. Influence of the thickness of the top-layer on the selectivity of the catalytic membranes during hydrogenation of nitrate. Pore size of the top-layer (nominal): 100 nm. Reference conditions — gas side hydrogen pressure: 4 bar. pH: 4.7. Temperature: 15°C. Residence time: 60 min.

the formation of the intermediate product nitrite is very low. A moderate increase of the selectivity to nitrogen with decreasing thickness of the top-layer can be noticed. However, given a total variation of the selectivity to nitrogen from 63 to 88%, this trend is by far not as clear as the decrease of activity witnessed by Fig. 13. The large scattering of the data suggests that other effects may contribute to the observed selectivity change as well. These include for instance the Pd:Sn ratio, which is very sensitive with respect to the catalytic performance. The scattering also indicates that the reproducibility of the preparation has to be improved.

3.3. Comparison with other approaches described in literature

The membranes having a catalytic top-layer of 20 μm thickness show an average specific activity of 0.9 mg nitrate removed per milligram palladium and hour, and an average nitrogen selectivity of 75%. It is instructive now to compare these values with typical results obtained from investigations on different catalyst systems and reactor types in literature, keeping in mind that such a comparison is not exact in a sense that equal operating conditions would have prevailed. First, the optimised powder-type Pd–Sn catalyst with a small grain size of 2–3 μm shows an average specific activity of 2.5 mg nitrate per milligram palladium and hour at a nitrogen selectivity of 96.2% when using hydrogen as reducing agent [14]. Such a catalyst cannot be used in commercial operation due to its very small particle size. Therefore, it was tried to transfer this excellent catalytic performance to catalyst types that may be used on an industrial scale. One approach is to immobilise the catalyst in a hydrogel (polyvinyl alcohol) [17], another one is to fill the catalyst into polymer hollow fibres [16]. The immobilisation in polyvinyl alcohol brought a loss of activity from 2.5 to 0.7 mg/mg h and, in addition, the selectivity to nitrogen was decreased to 74.9%. Moreover, for this type of catalyst rapid deactivation was observed, i.e., the third of several batch runs revealed already a decline of the activity by 50% compared to the initial value [17]. The immobilisation of the Pd–Sn catalyst in hollow fibres led to a low specific activity of 0.3 mg nitrate converted per milligram palladium and hour at a selectivity to nitrogen of 85% [16].

If one considers that the preparation of catalytic membranes by MOCVD or other techniques still has a large potential for optimisation, e.g. in terms of the metal dispersion, one can conclude from the comparison of the catalytic results given in this paper with literature data that the proposed concept of catalytic membranes separating gas and liquid flow indeed is

a promising approach for catalytic hydrogenation of nitrate. This concerns not only the fixation of an optimum catalyst composition in a membrane but also process engineering aspects, for example the possibility to tune the reaction rate by increasing the gas side hydrogen pressure [20].

4. Conclusion

The development of porous catalytic membranes for the reduction of nitrate in drinking water reported in this paper seems to offer interesting perspectives for a membrane-based catalytic denitrification process. These can be seen first of all in the use of membranes as catalyst support and hydrogen dosing unit in one single apparatus, and in avoiding to handle troublesome fine catalyst powders on an industrial scale. It has been shown that the membrane layer thickness has an influence mainly on the activity, whereas the selectivity seems to be affected in second place only. The thickness of the top-layer should not exceed 20 μm in order to avoid a loss of activity. However, the membranes prepared so far do not yet meet the desired selectivity and activity criteria. Therefore, additional work will be focussed on optimising the preparation, e.g. by MOCVD. A detailed characterisation of the membranes in terms of the particle size and the distribution of the active metals is required as well as a rigorous modelling of reaction and diffusion inside the membrane layers to facilitate the understanding of the system.

Acknowledgements

The authors wish to thank Mrs. M. Schorr for performing EPMA line scans and M. Jusek for carrying out pulse CO-chemisorption as well as XRD measurements. We also thank Prof. R. Schlögl and Dr. G. Mestl of Fritz-Haber-Institut, Berlin, for enabling TEM and XRD investigations and our partners G. Strukul, R. Gavagnin, G. Centi, M. Marella, M. Tomaselli, F. Luck and M. van Donk for many helpful discussions. Financial support by the European Community under contract No. BRPR-CT97-0420 is gratefully acknowledged.

References

[1] L.W. Canter, Nitrates in Groundwater, CRC Press, Boca Raton, FL, 1997.
[2] A. Kapoor, T.J. Viraraghavan, J. Environ. Eng. 123 (1997) 371.
[3] K.-D. Vorlop, T. Tacke, 'Chemie Ingenieur Technik' 61 (1989) 836.
[4] M. Sell, M. Bischoff, D. Bonse, Vom Wasser 79 (1992) 129.
[5] K.-D. Vorlop, Jahrbuch Biotechnol. 4 (1992) 307.
[6] G. Strukul, F. Pinna, M. Marella, L. Meregalli, M. Tomaselli, Catal. Today 27 (1996) 209.
[7] S. Hörold, K.-D. Vorlop, T. Tacke, M. Sell, Catal. Today 17 (1993) 21.
[8] U. Prüße, S. Hörold, K.-D. Vorlop, 'Chemie Ingenieur Technik' 69 (1993) 93.
[9] A. Pintar, M. Šetinc, J. Levec, J. Catal. 174 (1998) 72.
[10] M. Hähnlein, U. Prüße, S. Hörold, K.-D. Vorlop, 'Chemie. Ingenieur. Technik'. 69 (1997) 90.
[11] J. Wärnå, I. Turunen, T. Salmi, T. Maunula, Chem. Eng. Sci. 49 (1994) 5763.
[12] T. Tacke, K.D. Vorlop, 'Chemie Ingenieur Technik' 65 (1993) 1500.
[13] M. Hähnlein, Ph.D. Thesis, TU Braunschweig, 1999.
[14] U. Prüße, Ph.D. Thesis, TU Braunschweig, 1999.
[15] K. Lüdtke, K.-V. Peinemann, R.-D. Behling, J. Membr. Sci. 151 (1998) 3.
[16] M. Hähnlein, U. Prüsse, J. Daum, V. Morawsky, M. Kröger, M. Schröder, M. Schnabel, K.-D. Vorlop, in: B. Delmon, P.A. Jacobs, R. Maggi, J.A. Martens, P. Grange, G. Poncelet (Eds.), Studies in Surface Science and Catalysis, Vol. 118, Prep. Catal. VII, Elsevier, Amsterdam, 1998, p. 99.
[17] U. Prüße, V. Moravsky, A. Dierich, A. Vaccaro, K.-D. Vorlop, in: B. Delmon, P.A. Jacobs, R. Maggi, J.A. Martens, P. Grange, G. Poncelet (Eds.), Studies in Surface Science and Catalysis, Vol. 118, Prep. Catal. VII, Elsevier, Amsterdam, 1998, p. 137.
[18] O.M. Ilinitch, P.F. Cuperus, L.V. Nosova, E.N. Gribov, Catal. Today 56 (2000) 137.
[19] K. Daub, R. Dittmeyer, Proceedings of the 15th International Symposium on Chem. React. Eng. (ISCRE 15), Newport Beach, CA, September 13–16, 1998.
[20] K. Daub, G. Emig, M.-J. Chollier, M. Callant, R. Dittmeyer, Chem. Eng. Sci. 54 (1999) 1577.
[21] V. Bhaskaran, M.J. Hampden-Smith, T.T. Kodas, Chem. Vap. Deposition 3 (1997) 85.
[22] P. Atanasova, J. Wise, M. Fallbach, T. Kodas, M. Hampden-Smith, in: B. Delmon, P.A. Jacobs, R. Maggi, J.A. Martens, P. Grange, G. Poncelet (Eds.), Studies in Surface Science and Catalysis, Vol. 118, Prep. Catal. VII, Elsevier, Amsterdam, 1998.
[23] J.-C. Hierso, P. Serp, R. Feurer, P. Kalck, Appl. Organomet. Chem. 12 (1998) 161.
[24] C.R. Stillwell, Proceedings of the Seventh World Filtration Congress, Budapest, Hungary, May 1996.
[25] T. Tacke, Ph.D. Thesis, TU Braunschweig, 1991.